



Full-length article

Formation of diblock copolymer nanoparticles: Theoretical aspects

Yanyan Zhu^{a,b}, Bin Zheng^{c,e}, Liangshun Zhang^d, David Andelman^c, Xingkun Man^{a,b,*}

^a Center of Soft Matter Physics and its Applications, Beihang University, Beijing 100191, China

^b School of Physics, Beihang University, Beijing 100191, China

^c School of Physics and Astronomy, Tel Aviv University, Ramat Aviv 69978, Tel Aviv, Israel

^d Shanghai Key Laboratory of Advanced Polymeric Materials, Key Laboratory for Ultrafine Materials of Ministry of Education, School of Materials Science and Engineering, East China University of Science and Technology, Shanghai 200237, China

^e Wenzhou Institute, University of Chinese Academy of Sciences, Wenzhou, Zhejiang 325000, China



ARTICLE INFO

Keywords:

Block copolymer particles
Ellipsoidal particle
Onion-like spherical particle
Ginzburg-Landau free energy
Dynamic self-consistent field theory (DSCFT)

ABSTRACT

We explore the shape and internal structure of diblock copolymer (di-BCP) nanoparticles (NPs) by using the Ginzburg-Landau free-energy expansion and the dynamic self-consistent field theory (DSCFT). The self-assembly of di-BCP lamellae confined in emulsion droplets can form either ellipsoidal or onion-like NPs. The corresponding inner structure is a lamellar phase that is either perpendicular to the ellipsoid long axis (L_{\perp}) or forms a multi-layer concentric shell (C_{\parallel}), respectively. We focus on the effects of the interaction parameters between the A and B monomers χ , and polymer/solvent χ_{ps} , as well as the NP size on the nanoparticle shape and internal morphology. The aspect ratio (l_{AR}), defined as the length ratio between the long and short axes, is used to characterize the overall NP shape. Our results show that when the solvent is neutral towards the two blocks, the ratio l_{AR} increases as χ increases, indicating that the NP becomes more elongated. Likewise, decreasing χ_{ps} or increasing the NP size also results in a more elongated NP. Furthermore, as the solvent preference towards one of the A or B blocks increases, the NP undergoes a shape transition from a striped ellipsoid (L_{\perp}) to onion-like sphere (C_{\parallel}). Our results are in good agreement with previous experiments, and some of the predictions could be tested in future experiments.

1. Introduction

Polymeric nanoparticles (NPs) with well-controlled internal structures have attracted a large amount of interest due to their multiple applications [1–3]. The self-assembly of block copolymers (BCP) into droplets has been proven to be a useful method to produce NPs with well-defined shapes and internal morphologies [4–6]. Such NPs containing BCP are used in a wide range of applications such as drug delivery, smart coatings, catalysis and optical lenses [7–9]. From a fundamental viewpoint, the formation of BCP particles is related to the minimization of the interfacial energy of soft particles during the self-assembly process. Consequently, diverse particle shapes are formed under *soft confinement*, including onion-like spherical NPs [10,11], striped ellipsoidal NPs [12,13], conical shaped NPs [14,15], oblate NPs composed of cylindrical phases [16,17], and more. By soft confinement we mean situations where the interface between NP and surrounding solvent is soft and can be easily deformed. We illustrate in Fig. 1 two of the most common shapes of BCP particles that will be discussed

throughout our paper: (a) striped ellipsoidal shape (L_{\perp}); and, (b) an onion-like spherical shape (C_{\parallel}).

One of the current experimental challenges is to fabricate ellipsoidal BCP particles with precisely controlled shapes characterized by the particle aspect ratio (l_{AR}) and internal morphology, where the aspect ratio, l_{AR} , is defined as the ratio between the long and short axes of the ellipsoidal particle. Significant efforts have been devoted to address this challenge. Among experimental attempts to control the particle shape, we mention the addition of surfactants, inclusion of other solid-like NPs, and varying the solvent evaporation rate [18–20].

Kim and co-workers conducted a series of experiments on BCP particles. They systematically investigated the fabrication of such NPs with various shapes and inner structures. They found that the NP size [21], BCP molecular weight [22] as well as the Flory-Huggins interaction parameter [23] are the three key parameters that control the shape (l_{AR}) of ellipsoidal BCP particles. Moreover, the addition of surfactants, including length-controlled nanorod surfactants [24] or photo-responsive surfactants [25,26], can induce the transition of striped

* Corresponding author at: School of Physics, Beihang University, Beijing 100191, China.

E-mail address: manxk@buaa.edu.cn (X. Man).

ellipsoidal (L_{\perp}) NPs to onion-like spherical ($C_{||}$) NPs, due to the variation of the interfacial energy between the BCP particles and the solvent. On the theoretical side, phenomenological free-energies of BCP particles have been proposed [12,27,28] to explain these experimental findings. It was shown that the NP shape is determined by the competition between (i) the interfacial energy between the di-BCP two blocks, (ii) the entropic penalty due to chain stretching and bending, and (iii) the surface energy of BCP particles in contact with their surroundings (poor solvent).

In a separate study, Avalos et al. [29] presented experimental results of annealing BCP-NPs and developed a theoretical model based on the Cahn-Hilliard model to describe the morphological evolution of striped ellipsoids into onion-like spheres. They showed that as the temperature changes, the temperature-dependent Flory-Huggins parameter and the interface width vary accordingly, and eventually result in a morphology change. Chi et al. [30] studied the BCP self-assembly in soft confinement in poor solvent conditions using the simulated annealing method. They predicted different shapes and internal structures of BCP particles as function of the polymer-solvent interaction strength and BCP monomer concentration in solution. Recently, Zhu and co-workers showed that the BCP particles can undergo order-to-order morphological transformation from patchy particles to pupa-like (cocoon) or onion-like particles by varying the solvent selectivity and interfacial interaction [31–35].

Although BCP particles are easily obtained in experiments, at present there is a lack of rigorous theoretical description. Hence, a systematic theoretical study of the formation mechanism of BCP particles, and, in particular, the influence of these key experimental parameters (mentioned above) on the NP shape, is still highly desired. Such studies will not only enhance our understanding of how these parameters determine the final shape of BCP particles, but may also aid in the development of novel applications.

To address this challenge, we employ in the present work a Ginzburg-Landau free-energy and a dynamic self-consistent field theory (DSCFT) to study the self-assembly of BCP particles embedded in a poor solvent. Particularly, we focus on the effect of the AB block interaction parameter and the NP size. We also explore the symmetric and asymmetric interactions between the polymer blocks and the solvent, and their effect on the final shape and inner structure of BCP particles. We show that most of the experimental findings of lamellar-forming BCP particles can be captured by our model. Furthermore, we present several predictions on how experimental controllable parameters affect the final shape of the BCP particles.

Hereafter, the model based on the Ginzburg-Landau free-energy is introduced in Section 2. In Section 3, the calculated phase diagram separating NPs of distinct shapes in 2D is presented in terms of the interactions between different system components and the NP size, and then, we show the 3D calculations using DSCFT. Finally, Section 4 contains a comparison between our predictions and existing

experiments as well as other models, followed by some conclusions and future prospects.

2. Model

We study the equilibrium shape of diblock copolymer NPs embedded in a solution by using the Ginzburg-Landau free-energy [36,37]. The system we model is a mixture of three components: the A and B components of di-BCPs and a solvent. The incompressibility condition is $\phi_A + \phi_B + \phi_S = 1$, where ϕ_A , ϕ_B , and ϕ_S are the volume fractions of the A and B monomers and the solvent, respectively.

Two order parameters are introduced for convenience,

$$\begin{aligned} \rho &= \phi_A + \phi_B, \\ \phi &= \phi_A - \phi_B \end{aligned} \quad (1)$$

where ρ is the total BCP volume fraction, and ϕ is the local concentration difference between the A and B monomers.

In the grand-canonical ensemble, the Ginzburg-Landau free-energy of the AB di-BCP system is written as [37]:

$$\begin{aligned} \frac{F(\phi, \rho)}{k_B T} &= \int d^3 \mathbf{r} \left[-\frac{\chi}{2} \phi^2 + \frac{\chi_{ps}}{2} \rho(1 - \rho) + \nu_{\phi\rho} \phi(1 - \rho) - \mu_{\phi} \phi - \mu_{\rho} \rho \right. \\ &\quad \left. + \frac{\rho + \phi}{2} \ln(\rho + \phi) + \frac{\rho - \phi}{2} \ln(\rho - \phi) + (1 - \rho) \ln(1 - \rho) \right. \\ &\quad \left. + \frac{H}{2} [(\nabla^2 + q_0^2) \phi]^2 + K(\nabla \rho)^2 \right] \end{aligned} \quad (2)$$

In the above free energy, the first three terms are the interaction terms, where $\chi = 2n_c N(\chi_{AB} - \chi_c)$ denotes the interaction between the A and B monomers, with $n_c = 1/(Na^3)$ being the polymer density, a the monomer size. And N is the degree of polymerization of a whole BCP chain, χ_{AB} is the Flory-Huggins parameter between A and B monomers, and $\chi_c = 10.495/N$ is the value at the critical point (ODT). χ_{ps} is the interaction parameter between solvent and polymer, $\nu_{\phi\rho}$ denotes the preference interaction of solvent towards either the A or B monomers, and μ_{ϕ} and μ_{ρ} are the corresponding chemical potentials. The chemical potential has two effects: (i) it is used to regulate the average value of the total polymer density ρ , and (ii) it is used to determine whether the system will have two coexisting phases or just one phase at equilibrium. The next term is the ideal entropy of mixing, while the H -term induces a modulated phase in the AB relative concentration ϕ . The H prefactor is the modulation strength parameter and $q_0 \sim 1/R_g$ is the most dominant wavenumber [38]. The last item, parameterized by the K prefactor, characterizes the stiffness of the interface between the polymer and the solvent [39].

In order to analyze the formation mechanism of BCP ellipsoidal NPs, we focus on two separate energy terms of the full Ginzburg-Landau free-energy, Eq. (2). The first one is the polymer free-energy F_p that includes

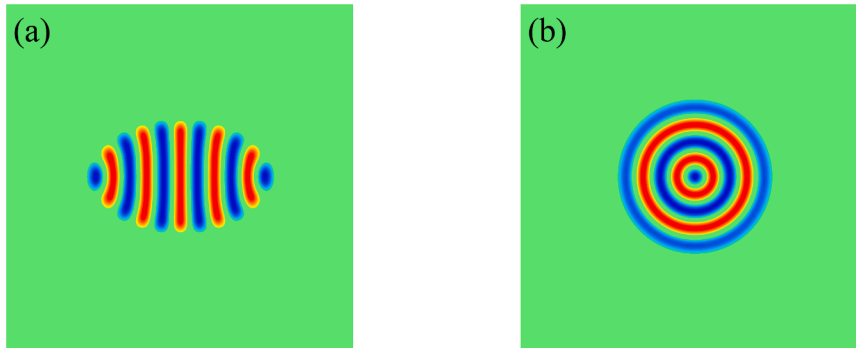


Fig. 1. Two typical microphases of AB diblock copolymer nanoparticles embedded in a poor solvent solution. (a) Striped ellipsoidal NP. (b) Onion-like spherical NP. A-rich lamellae are colored red and B-rich are blue. (For interpretation of the references to colour in this figure legend, the reader is referred to the web version of this article.)

both enthalpy and entropy of the polymer chains,

$$F_P = -\frac{\chi}{2}\phi^2 + \frac{\rho + \phi}{2}\ln(\rho + \phi) + \frac{\rho - \phi}{2}\ln(\rho - \phi) \quad (3)$$

The second term is the polymer-solvent interfacial energy E_{PS} ,

$$E_{PS} = \frac{\chi_{ps}}{2}\rho(1 - \rho) + \nu_{\phi\rho}\phi(1 - \rho) \quad (4)$$

We will show that the BCP particle equilibrium shape is determined mainly by the competition between these two terms of the full free-energy, Eq. (2).

We use the conjugate gradient (CG) method to minimize the Ginzburg-Landau free-energy, Eq. (2), in order to obtain the equilibrium density distribution of each component. Most of our numerical calculations are performed in a two-dimensional (2D) box ($L_x \times L_y$) with a spatial grid $\Delta x = \Delta y = 0.05$. We use the value of $K = 0.05$ in the neutral solvent case, and $K = 3$ when the solvent has a preference towards one of the two blocks. Here, as the interaction between the polymer and solvent becomes stronger, a larger K value is needed to maintain the shape of the NP. In all calculations, the chemical potentials are $\mu_\phi = 0$, $\mu_\rho = -0.01$, and $H = 3$. In addition, we set the wavenumber $q_0 = 1$ (in dimensionless units). All lengths are expressed in units of L_0 , which is the fixed bulk natural periodicity of the lamellar phase $L_0 \equiv 2\pi/q_0$. We also conduct three-dimensional (3D) calculations on the formation of NPs by using a 3D dynamic self-consistent field theory (DSCFT). More details of our 3D DSCFT calculations are presented in Section 3.

3. Results

It is known from experiments that the lamellar phase of BCP solution can form either ellipsoidal or onion-like NPs (Fig. 1). The lamellar order is usually perpendicular to the long axis for ellipsoidal NPs (L_\perp), while concentric shell structures ($C_{||}$) are formed for onion-like NPs. The equilibrium shape of BCP particles is mainly determined experimentally [23,28,40] by the AB monomer interaction parameter χ , the polymer/solvent interaction parameter χ_{ps} , the preference of the solvent towards one of the two components $\nu_{\phi\rho}$, and the size of the NPs. Therefore, we mainly focus on the effects of these experimental controllable parameters on the shape and inner structure of the BCP particles.

3.1. Ellipsoidal particles (L_\perp)

When the solvent preference towards the A and B components is neutral, $\nu_{\phi\rho} = 0$, ellipsoidal NPs are usually formed. In this subsection, we study the effect of the parameters χ , χ_{ps} , and the NP size on the equilibrium shape of the BCP particles, where for ellipsoidal NPs, the aspect ratio l_{AR} between the major and minor axes serves as the shape parameter.

3.1.1. The effect of χ and χ_{ps} on the NP shape

We first explore the effect of the interaction parameter between the A and B components, χ , and the interaction parameter between polymer and solvent, χ_{ps} , on the equilibrated l_{AR} of the BCP particles. For a given set of (χ_{ps}, χ) , we calculated the equilibrium $l_{AR} = a/b$ by fixing the particle size $S = \pi ab = 4\pi L_0^2$, where a, b are the ellipsoid principal axes (in two-dimensions), and L_0 is the natural periodicity of the lamellar phase. The initial NP state is chosen such that the NP long axis is always an integer multiple of L_0 . This is done in order to ensure the commensurability matching between the particle size and the domain spacing, thereby limiting the confinement effect on the final NP shape. More specifically, (a, b) are chosen initially to have discrete values: $(2L_0, 2L_0)$; $(2.5L_0, 1.6L_0)$; $(3L_0, 1.33L_0)$; $(3.5L_0, 1.14L_0)$, and $(4L_0, L_0)$, corresponding to an aspect ratio, $l_{AR} = 1, 1.56, 2.26, 3.07$ and 4 , and an integer number of lamellae inside the NP: $4, 5, 6, 7$, and 8 , respectively. We then compare

the calculated free energy of the NP for the various initial conditions, and the chosen l_{AR} corresponds to the minimum free-energy for this particle size. Note that the particle evolves spontaneously to an equilibrated l_{AR} , which is somewhat different from the initial one. The interface between the NP and the surrounding bad solvent is a free interface that self-adjusts with respect to the system conditions. By considering the l_{AR} values, the system behavior can be divided into four regions as shown in Fig. 2.

Fig. 2 shows the phase diagram in terms of distinct values of the l_{AR} in the (χ_{ps}, χ) plane. As can be seen in the phase diagram presented in the figure for fixed χ , l_{AR} decreases when χ_{ps} increases, while for fixed χ_{ps} , l_{AR} increases as χ increases. The phase diagram also shows that large values of χ are needed to get more elongated NP in the large χ_{ps} region. In other words, the particle l_{AR} value can be increased by increasing χ or decreasing χ_{ps} .

Fig. 3a shows that for $\chi = 2.6$ and $\chi_{ps} = 7.0$, the free energy has a minimum at $l_{AR} = 2.59$, indicating the formation of an ellipsoidal NP. To understand why the NPs have an equilibrium l_{AR} for a given (χ_{ps}, χ) , we calculate two separate contributions to the total free-energy, F_P and E_{PS} , as function of l_{AR} and show them in Fig. 3b. Here, F_P is the polymer free-energy, including the enthalpy and entropy, and E_{PS} is the polymer/solvent interfacial energy. Our results indicate that for fixed values of the (χ_{ps}, χ) parameters, as l_{AR} increases, F_P decreases while E_{PS} increases.

The decrease in F_P as l_{AR} increases is due to the lamellar orientation that is perpendicular to the long axis. The BCPs are more sensitive to the confinement along the long axis than along the short axis. One of our conclusions is that the confinement becomes weaker when the ellipsoid long axis becomes longer. Namely, larger l_{AR} results in less confinement of the BCP lamellae. However, when l_{AR} increases, the polymer/solvent interfacial energy increases, resulting in an increase of E_{PS} . In other words, F_P tends to elongate the NP, while E_{PS} prefers to make it more spherical. It is mainly the balance between these two terms that determines the final NP shape. As F_P is always negative (Fig. 3b), the effect of F_P on the NP shape is stronger when its value is smaller. On the other hand, as E_{PS} is always positive, its constraining effect on the final shape is stronger when its value is larger.

After understanding why the system has a preferred aspect ratio, l_{AR} , for a given set of χ and χ_{ps} , we turn to the effect of χ on the l_{AR} . The phase diagram in Fig. 2 shows that as χ increases from $\chi = 2.2$ to $\chi = 3.4$, l_{AR} increases accordingly. We analyze such behavior by exploring in Fig. 4 the dependence of F_P and E_{PS} on χ , where it is shown that F_P decreases and E_{PS} increases a little as χ increases. This indicates that increasing χ strongly enhances the elongation effect of F_P , while the constraining effect of E_{PS} causes the NP to become slightly more spherical. Therefore, as χ increases, F_P wins over E_{PS} and the NP becomes overall more elongated. We also employ a 3D dynamic self-consistent field theory (DSCFT) to explore the shape of 3D droplet and confirm this trend, more details of the 3D calculations can be seen in the Section 3.3.

On the other hand, an inverse tendency can be seen in the effect of χ_{ps} on l_{AR} , l_{AR} decreases when χ_{ps} increases. The dependency of E_{PS} and F_P on χ_{ps} is shown in Fig. 5a. It elucidates that upon increasing χ_{ps} , F_P increases and E_{PS} decreases. Hence, by increasing F_P , the NP becomes more spherical, while decreasing E_{PS} makes the NP more elongated. By varying the χ_{ps} value, the absolute change in the two energy terms is almost the same, i.e., E_{PS} decreases while F_P increases by roughly the same amount.

In Fig. 5b, we plot the dependence of ΔF_P and ΔE_{PS} on l_{AR} for $\chi_{ps} = 7.0$ and 7.5 , where $\Delta F_P = F_P(l_{AR}) - F_P^{ref}$, is the difference between $F_P(l_{AR})$ and a reference state of F_P^{ref} . Similarly, $\Delta E_{PS} = E_{PS}(l_{AR}) - E_{PS}^{ref}$. The reference state has the smallest value of l_{AR} (roughly 1), Fig. 5b shows that ΔE_{PS} is closer for these two χ_{ps} values, while ΔF_P is smaller for $\chi_{ps} = 7.0$ than for $\chi_{ps} = 7.5$. This indicates that dependence of the interfacial energy E_{PS} on l_{AR} almost does not change as χ_{ps} increases, but the effect on F_P is weaker for $\chi_{ps} = 7.5$ than for $\chi_{ps} = 7.0$. As a result, the NP

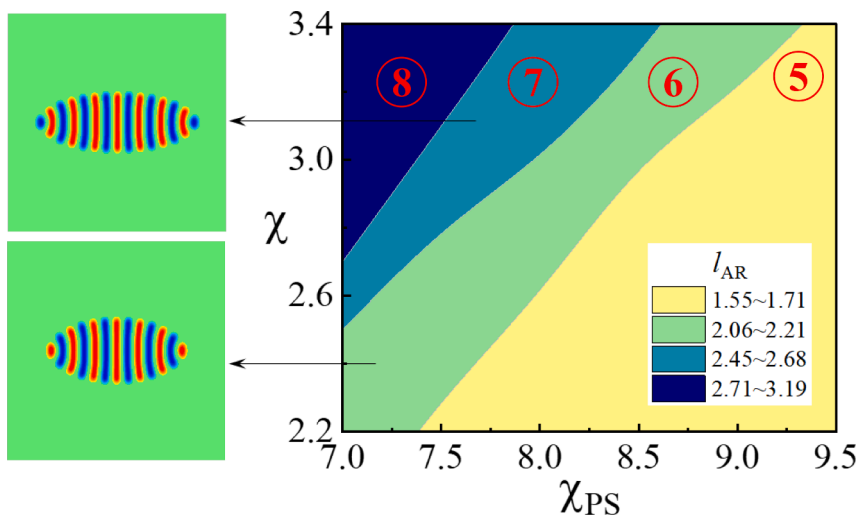


Fig. 2. The phase diagram plotted in the (χ_{PS}, χ) parameter plane for a BCP particle embedded in a po solvent. The equilibrated l_{AR} range is divided into four colored regions, shown in the phase diagram as yellow (5), green (6), green-blue (7) and dark blue (8), where the number in parenthesis corresponds to the number of BCP layers within the particle varying from 5 to 8. The deeper the color is, the larger is l_{AR} (see legend). Other parameter values are: $\nu_{\phi\text{p}} = 0$, $H = 3$, and $K = 0.05$. The box size here and in subsequent figures is 10×10 in units of $L_0 = 2\pi/q_0 \approx 3.22R_g$. (For interpretation of the references to colour in this figure legend, the reader is referred to the web version of this article.)

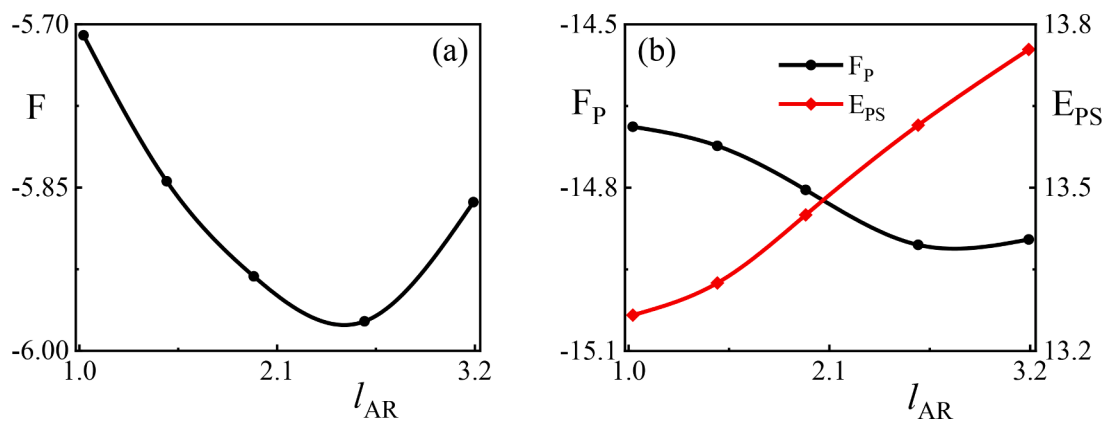


Fig. 3. (a) Dependence of the total free energy F on the aspect ratio, l_{AR} . (b) Separate plots of the polymer energy F_{P} (black line) and interfacial energy E_{PS} (red line) as function of l_{AR} . We calculate a few discrete values of l_{AR} , and the continuous lines serve as a guide to the eye. Other parameter values are: $\chi = 2.6$, $\chi_{\text{PS}} = 7.0$, $\nu_{\phi\text{p}} = 0$, $H = 3$, and $K = 0.05$. (For interpretation of the references to colour in this figure legend, the reader is referred to the web version of this article.)

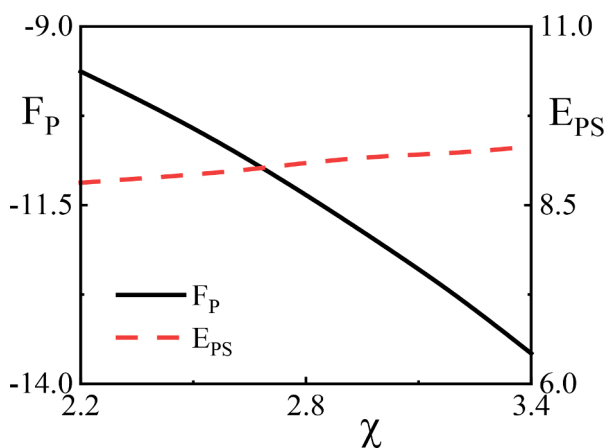


Fig. 4. The dependence of F_{P} (solid black line) and E_{PS} (dashed red line) on χ for NPs with five BCP layers inside having an area $S = 4\pi L_0^2$ and initial $l_{\text{AR}} = 1.56$. Other parameter values are: $\chi_{\text{PS}} = 8.0$, $\nu_{\phi\text{p}} = 0$, $H = 3$, and $K = 0.05$. (For interpretation of the references to colour in this figure legend, the reader is referred to the web version of this article.)

becomes less elongated as χ_{PS} increases.

3.1.2. The size effect on the NP shape

In addition to varying χ and χ_{PS} , we also investigate the dependence of the NP final shape on its size. In our calculations, the final NP size changes just a little from its initial size. Hence, we can adjust the initial condition in order to get the desired NP size. The area of the ellipse $S = \pi ab$, where a and b are the two principal axes, is used to characterize the NP size in 2D. For a given area S , we calculate the BCP-NPs free-energy for various $l_{\text{AR}} = a/b$. The l_{AR} that corresponds to the minimum free energy is taken as the equilibrium one. Fig. 6a shows two equilibrium shapes of BCP particles for $S = 9.42$ and 19.63 with two corresponding equilibrated $l_{\text{AR}} = 1.47$ and 2.03 . The number of lamellae inside the NP is 4 and 7, respectively. The dependence of l_{AR} for the particle size S is shown in Fig. 6b, and in Fig. 6c one sees that F_{P} decreases while E_{PS} increases a little as S increases. This indicates that for NP sizes, F_{P} has a more dominant contribution than E_{PS} on the equilibrium shape. Therefore, l_{AR} increases as the size increases, as in clearly seen in Fig. 6b.

3.2. Onion-like spherical particles (C_{\parallel})

So far we discussed the neutral solvents having $\nu_{\phi\text{p}} = 0$. The resulting NP has an ellipsoidal shape (in 2D) with inner BCP lamellae that are perpendicular to the long axis (L_{\perp}). This phenomenon is also seen in experiments. Let us now consider solvents that have a preference to-

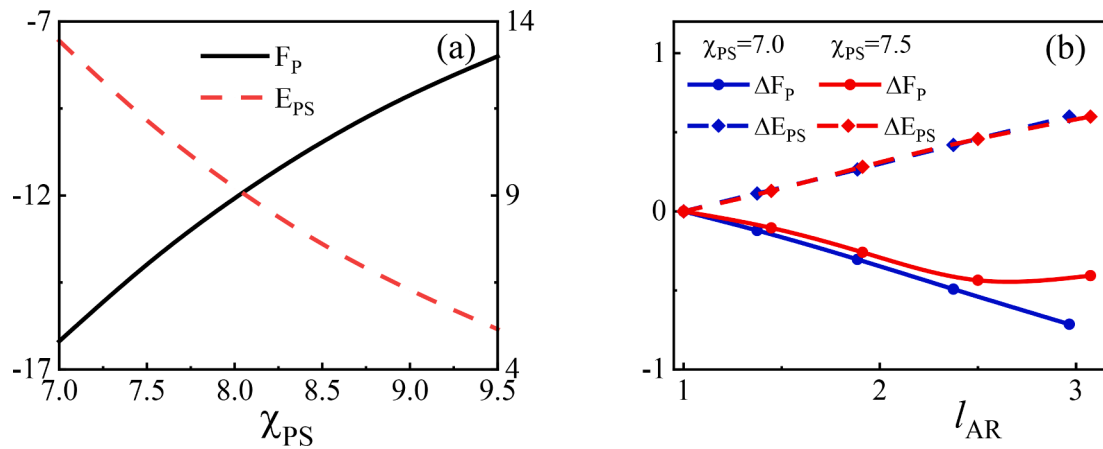


Fig. 5. (a) F_P (solid black line) and E_{PS} (dashed red line) as function of the polymer-solvent interaction parameter, χ_{PS} , for NPs with five BCP layers inside with an area $S = 4\pi L_0^2$ and initial $l_{AR} = 1.56$. (b) Dependence of ΔF_P (solid line) and ΔE_{PS} (dashed line) on l_{AR} for $\chi_{PS} = 7.0$ (blue line) and $\chi_{PS} = 7.5$ (red line), where $\Delta F_P = F_P(l_{AR}) - F_P^{ref}$ and $\Delta E_{PS} = E_{PS}(l_{AR}) - E_{PS}^{ref}$. Other parameter values are: $\chi = 3.0$, $\nu_{\phi\phi} = 0$, $H = 3$, and $K = 0.05$. The reference states of both F_P^{ref} and E_{PS}^{ref} have the smallest value of l_{AR} , which is roughly 1. (For interpretation of the references to colour in this figure legend, the reader is referred to the web version of this article.)

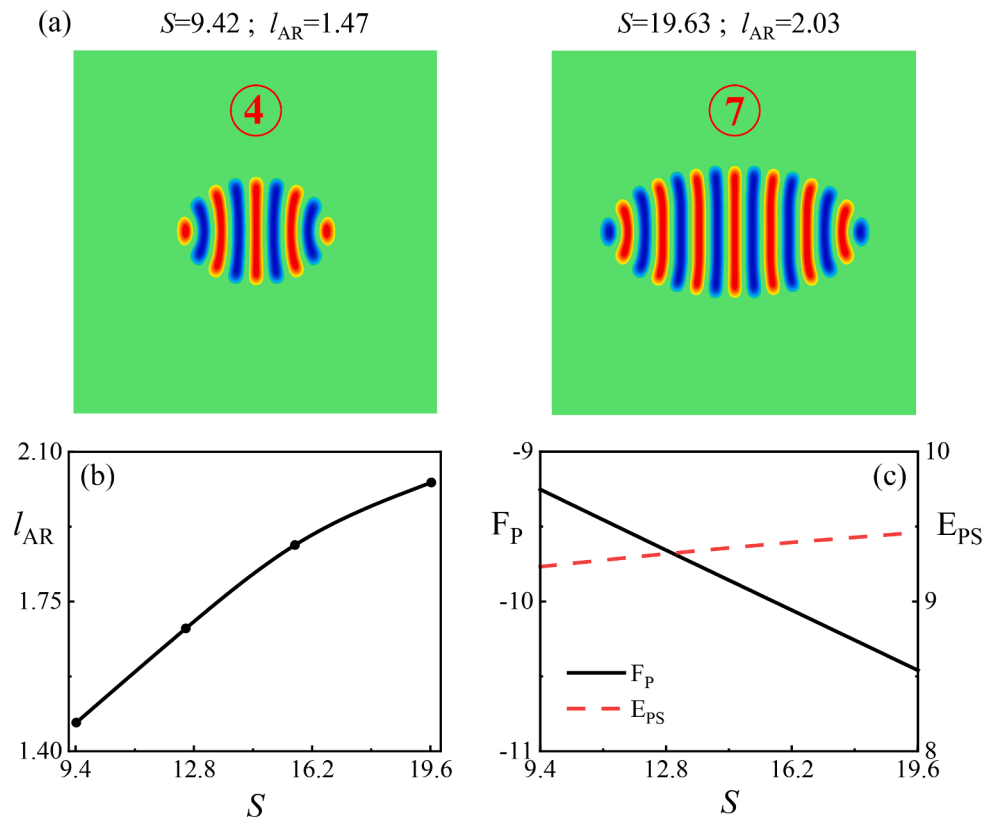


Fig. 6. (a) The equilibrated NP shapes for different areas, S , in units of L_0^2 , and their corresponding aspect ratio l_{AR} from left to right are: $S = 9.42$, $l_{AR} = 1.47$ (4 layers); and $S = 19.63$, $l_{AR} = 2.03$ (7 layers). (b) Dependence of the aspect ratio l_{AR} on the area S . (c) Dependence of F_P and E_{PS} on the area S . We calculate a few discrete values of S , and the continuous lines serve as a guide to the eye. Other parameter values are: $\chi = 2.2$, $\chi_{PS} = 8.0$, $\nu_{\phi\phi} = 0$, $H = 3$, and $K = 0.05$.

wards one of the two blocks, *i.e.*, $\nu_{\phi\phi} \neq 0$. Experiments [25,40] have shown that when the solvent prefers, say, the B component, an onion-like structure ($C_{||}$) with a B-shell on the NP perimeter is formed. Clearly, the opposite occurs if the solvent prefers the A component resulting in an onion-like structure ($C_{||}$) with an A-shell on its perimeter, in agreement with our calculations. Next, we would like to investigate in more detail how the onion-like structure appears when $\nu_{\phi\phi}$ becomes large enough.

Fig. 7a shows that by increasing the preference of $\nu_{\phi\phi}$ from 0 to 3.0,

the NP shape changes first from an ellipsoidal to more spherical, and then to an onion-like sphere. At the same time, the inner structure changes from lamellae perpendicular to the long NP axis (L_{\perp}) to a structure with concentric shells ($C_{||}$). For given values of χ and χ_{PS} , a critical value of $\nu_{\phi\phi} = \nu^*$ is needed to induce a structural transition from L_{\perp} to $C_{||}$. Fig. 7b shows that for $\chi = 2.2$, the critical value ν^* at the transition increases as χ_{PS} increases. The transition line, shown in Fig. 7b, separates an upper $C_{||}$ phase from a lower L_{\perp} phase.

The change in the NP shape and its inner structure as a function of $\nu_{\phi\phi}$

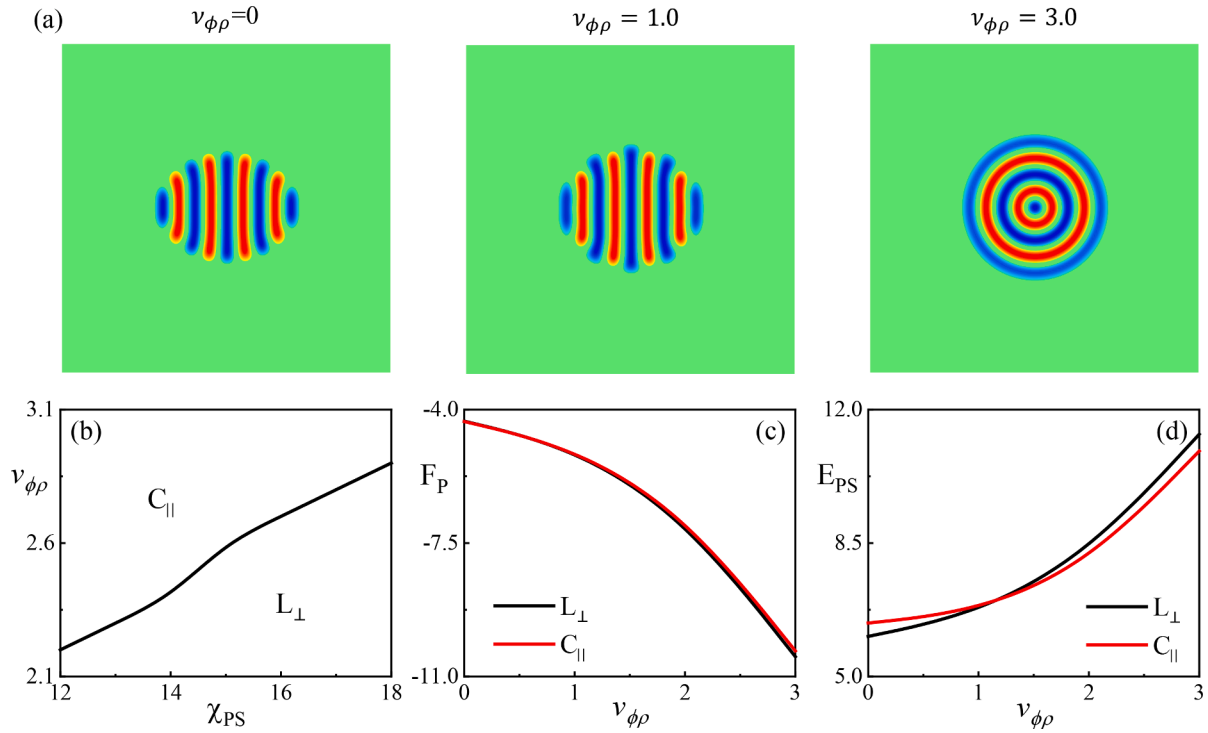


Fig. 7. (a) The equilibrium shape of an NP as the solvent preference increases. From left to right, the values of $\nu_{\phi\rho}$ are: $\nu_{\phi\rho} = 0, 1.0,$ and 3.0 . (b) The C_{\parallel} to L_{\perp} phase diagram in the $(\chi_{PS}, \nu_{\phi\rho})$ plane for $\chi = 2.2$. F_P in (c) and E_{PS} in (d) are plotted as function of $\nu_{\phi\rho}$ for $\chi = 2.2$ and $\chi_{PS} = 12.0$. In addition, $H = 3$ and $K = 3$.

can also be observed by the dependency of F_P and E_{PS} on $\nu_{\phi\rho}$, as shown in Fig. 7c and d. F_P is almost the same for the L_{\perp} and C_{\parallel} structures, while E_{PS} turns to be larger for the L_{\perp} phase than for the C_{\parallel} as $\nu_{\phi\rho}$ increases. This means that E_{PS} is the key term for determining the shape and inner structure of NPs. As $\nu_{\phi\rho}$ increases, E_{PS} of the C_{\parallel} phase decreases, and the NP shape changes from L_{\perp} to C_{\parallel} . Note that the spherical L_{\perp} is an intermediate structure of this transition.

3.3. 3D DSCFT calculations

As the 2D model may have limited applicability to three dimensional (3D) experiments, we additionally employ a 3D dynamic self-consistent field theory (DSCFT) to study the effect of the Flory-Huggins interaction between AB diblock on the NP shape [41–43]. We consider a system composed of symmetric AB di-BCPs ($f = 0.5$) and homopolymers (denoted as C) that can be regarded as a bad solvent for the di-BCPs [44]. The size of the 3D simulation box is $L_x \times L_y \times L_z = 16R_g \times 9R_g \times 9R_g$, where R_g is the chain radius of gyration. In all simulations, the volume fraction of di-BCP is set to be 0.1, and the ratio of chain length between C

and di-BCP is chosen as 0.3. The various Flory-Huggins interactions between the three components (A, B, and C) are denoted as χ_{AC} , χ_{BC} and χ_{AB} . We take $N\chi_{AC} = N\chi_{BC} = 20$ to mimic the situation of di-BCPs being surrounded by a bad solvent, and then focus on the dependence of equilibrium l_{AR} on $N\chi_{AB}$. For all cases, we only change $N\chi_{AB}$ and the NP evolves spontaneously into a striped ellipsoid (L_{\perp}).

Fig. 8 shows that the NP equilibrium shape differs as $N\chi_{AB}$ changes. More specifically, Fig. 8a exhibits two typical equilibrium shapes of NPs for $N\chi_{AB} = 15$ and 36, with corresponding $l_{AR} = 1.14$ and 1.47, respectively. In this 3D calculation, l_{AR} is the length ratio between the long and short axes of the prolate ellipsoid. Fig. 8b shows that l_{AR} increases as $N\chi_{AB}$ increases. This is consistent with our 2D results.

4. Discussion and conclusions

4.1. Comparison with experiments

Our study of the BCP particle formation mechanism was inspired by a recent series of experimental studies [21,23]. Shin et al. [21] have

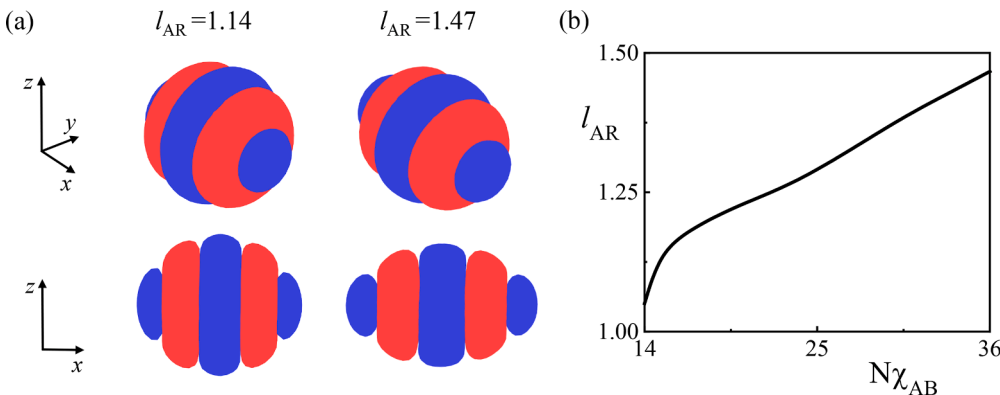


Fig. 8. (a) The calculated 3D equilibrium shape of NPs for various Flory-Huggins interactions. (left) The Flory-Huggins interaction $N\chi_{AB}$, the aspect ratio l_{AR} and the natural periodicity of lamellar phase L_0 are: $N\chi_{AB} = 15$, $l_{AR} = 1.14$, $L_0 = 3.375R_g$; and (right) $N\chi_{AB} = 36$, $l_{AR} = 1.47$, $L_0 = 4.125R_g$. In both cases we have two layers. The top row shows the 3D overall shape, while the bottom row shows the corresponding side-view. (b) The dependence of l_{AR} on the Flory-Huggins interaction $N\chi_{AB}$. The size of simulation box is $16 \times 9 \times 9$ in units of R_g , and $N\chi_{AC} = N\chi_{BC} = 20$.

shown that the NP aspect ratio l_{AR} can be controlled by tuning the NP size. They employed a membrane device made of Shirasu porous glass (SPG) to generate monodisperse NPs made from PS-*b*-PB block copolymers with different NP diameters. They found that l_{AR} increases as the NP size increases, which is in good agreement with our predictions shown in Fig. 6. The dependence of l_{AR} on the NP size can be attributed to the fact that increasing the NP size enhances the contribution of the bulk energy, while it decreases the surface energy due to the reduced surface area/volume ratio. The bulk energy includes mainly the polymer free energy (F_p in our calculations). This can be clearly seen in our work as increasing l_{AR} can decrease F_p (see Fig. 3b). For the L_{\perp} phase, the lamellae only feel the confinement along the long axis. Larger l_{AR} values imply that less confinement is applied to the BCP lamellar phase. In other words, lamellar BCPs prefer to form elongated NPs with inner lamellae perpendicular to the long axis (L_{\perp}).

Shin and co-workers [23] applied various type of di-BCP to generate NPs with different Flory-Huggins parameter, χ_{AB} . Their study included PS_{34k}-*b*-PB_{25k}, PS_{16k}-*b*-PDMS_{17k} and PS_{10k}-*b*-P4VP_{10k} with $\chi_{AB} = 0.04$, 0.21 and 0.53, respectively. They found that l_{AR} increases as χ_{AB} increases for the above series of di-BCP. Our results are consistent.

4.2. Comparison with other models

Our results on the dependence of the NP shape on χ and on the NP size are in qualitative agreement with the theoretical analysis of Ku et al. [28] The latter was based on a phenomenological coarse-grained free-energy. In their work, the proposed free-energy is composed of four terms: the interfacial energy between AB blocks, the stretching energy of di-BCP chains, the bending energy of curved lamellae, and the surface energy at the NP/solvent interface. The first three terms are the bulk energy, while the last term is the polymer/solvent interfacial energy. Such a phenomenological free-energy shows that when l_{AR} increases, both the AB interfacial and bending energies decrease, whereas the polymer/solvent surface energy increases. Moreover, when the NP size increases, the bulk energy increases, while the surface energy decreases, resulting in an increase of l_{AR} . Their free energy also shows that the bulk energy increases as the interaction between AB diblocks increases. Therefore, when χ increases, l_{AR} tends to increase in order to reduce the bulk energy. This is in accord with experimental observations as well as with our results that demonstrated that l_{AR} increases for BCPs with larger χ .

4.3. Concluding remarks

We systematically studied the mechanism of NP formation from diblock copolymers. Our results indicate that the BCP particle equilibrium shape is mainly determined by the competition between the polymer free-energy F_p and the polymer-solvent interfacial energy E_{ps} . We show that lamellar-forming BCPs prefer ellipsoidal NPs with inner lamellae perpendicular to the long axis (the L_{\perp} structure), while the solvent preference to one of the two blocks is causing the formation of onion-like NPs with inner lamellae arranged as concentric shells (the C_{\parallel} structure). When the solvent is neutral towards the two blocks, more elongated ellipsoidal NPs are obtained by increasing the AB interaction parameter χ , or by either decreasing the polymer/solvent interaction parameter χ_{ps} , or increasing the NP size.

On the other hand, when the solvent has a preference towards one of the two blocks, increasing the strength of this preference induces a transition in the NP shape first from ellipsoidal to spherical, and finally to onion-like. In a corresponding manner, the inner structure changes from lamellae perpendicular to the long axis to concentric shells. Our results not only are consistent with the current experimental findings, but also predict yet unexplored effects of how the equilibrium shape of BCP particles depends on experimental controlled parameters.

In this work, we studied BCP forming nanoparticles for which the

BCPs have a lamellar phase in the bulk and the NP shape is mainly ellipsoidal (both in 2D and 3D systems), the main results of 2D system are confirmed by a 3D DSCFT calculations. BCPs with a cylindrical structure in the bulk have been used in the fabrication of nanoparticles. The resulting NPs have an oblate shape and attracted much attention [3, 16, 23, 28]. We can also use Ginzburg-Landau equation to investigate the case of hexagonal phase inside NPs, which can be described by $\phi(x, y) = \phi_q \cos(q_0 x) + \phi_q \cos\left(q_0 \frac{\sqrt{3}y-x}{2}\right) + \phi_q \cos\left(-q_0 \frac{\sqrt{3}y+x}{2}\right)$, together with the chemical potential, $\mu_{\phi} \neq 0$. We leave these more elaborate calculations to future studies. We hope that the theoretical results presented in this work can serve as a useful guide for future experiments as well as towards applications for nanoparticles form from block copolymers.

Declaration of Competing Interest

The authors declare that they have no known competing financial interests or personal relationships that could have appeared to influence the work reported in this paper.

Acknowledgement

This work was supported in part by grants No. 21822302 of the National Natural Science Foundation of China (NSFC), and the NSFC-ISF Research Program, jointly funded by the NSFC under grant No. 21961142020 and the Israel Science Foundation (ISF) under grant No. 3396/19, and ISF grant No. 213/19. We also acknowledge the support by the High Performance Computing Center of Beihang University.

References

- [1] A.-C. Shi, B. Li, Self-assembly of diblock copolymers under confinement, *Soft Matter* 9 (2013) 1398–1413, <https://doi.org/10.1039/C2SM27031E>.
- [2] K.H. Ku, J.M. Shin, H. Yun, G.-R. Yi, S.G. Jang, B.J. Kim, Multidimensional design of anisotropic polymer particles from solvent-evaporative emulsion, *Adv. Funct. Mater.* 28 (2018) 1802961, <https://doi.org/10.1002/adfm.201802961>.
- [3] J.J. Shin, E.J. Kim, K.H. Ku, Y.J. Lee, C.J. Hawker, B.J. Kim, 100th Anniversary of macromolecular science viewpoint: block copolymer particles: tuning shape, interfaces, and morphology, *ACS Macro Lett.* 9 (2020) 306–317, <https://doi.org/10.1021/acsmacrolett.0c00020>.
- [4] S.J. Jeon, G.-R. Yi, S.M. Yang, Cooperative assembly of block copolymers with deformable interfaces: toward nanostructured particles, *Adv. Mater.* 20 (2008) 4103–4108, <https://doi.org/10.1002/adma.200801377>.
- [5] I. Wyman, G. Njikang, G. Liu, When emulsification meets self-assembly: the role of emulsification in directing block copolymer assembly, *Prog. Polym. Sci.* 36 (2011) 1152–1183, <https://doi.org/10.1016/j.progpolymsci.2011.04.005>.
- [6] M.P. Kim, G.R. Yi, Nanostructured colloidal particles by confined self-assembly of block copolymers in evaporative droplets, *Front. Mater.* 2 (2015) 1, <https://doi.org/10.3389/fmats.2015.00045>.
- [7] A. Fernández-Nieves, G. Cristobal, V. Garcés-Chávez, G.C. Spalding, K. Dholakia, D. A. Weitz, Optically anisotropic colloids of controllable shape, *Adv. Mater.* 17 (2005) 680–684, <https://doi.org/10.1002/adma.200401462>.
- [8] K.H. Ku, M.P. Kim, K. Paek, J.M. Shin, S. Chung, S.G. Jang, W.S. Chae, G.-R. Yi, B. J. Kim, Multicolor emission of hybrid block copolymer-quantum dot microspheres by controlled spatial isolation of quantum dots, *Small* 9 (2013) 2667–2672, <https://doi.org/10.1002/sml.201202839>.
- [9] K.H. Ku, J.M. Shin, M.P. Kim, C.H. Lee, M.K. Seo, G.-R. Yi, S.G. Jang, B.J. Kim, Size-controlled nanoparticle-guided assembly of block copolymers for convex lens-shaped particles, *J. Am. Chem. Soc.* 136 (2014) 9982–9989, <https://doi.org/10.1021/ja502075f>.
- [10] N. Saito, R. Takekoshi, R. Nakatsuru, M. Okubo, Effect of stabilizer on formation of “onionlike” multilayered polystyrene-block-poly(methyl methacrylate) particles, *Langmuir* 23 (2007) 5978–5983, <https://doi.org/10.1021/la063654f>.
- [11] T. Tanaka, N. Saito, M. Okubo, Control of layer thickness of onionlike multilayered composite polymer particles prepared by the solvent evaporation method, *Macromolecules* 42 (2009) 7423–7429, <https://doi.org/10.1021/ma901100n>.
- [12] S.G. Jang, D.J. Audus, D. Klinger, D.V. Krogstad, B.J. Kim, A. Cameron, S.W. Kim, K.T. Delaney, S.M. Hur, K.L. Killips, G.H. Fredrickson, E.J. Kramer, C.J. Hawker, Striped, ellipsoidal particles by controlled assembly of diblock copolymers, *J. Am. Chem. Soc.* 135 (2013) 6649–6657, <https://doi.org/10.1021/ja4019447>.
- [13] S. Lee, J.J. Shin, K.H. Ku, Y.J. Lee, S.G. Jang, H. Yun, B.J. Kim, Interfacial instability-driven morphological transition of prolate block copolymer particles: striped football, larva to sphere, *Macromolecules* 53 (2020) 7198–7206, <https://doi.org/10.1021/acs.macromol.0c01004>.
- [14] R. Deng, S. Liu, F. Liang, K. Wang, J. Zhu, Z. Yang, Polymeric janus particles with hierarchical structures, *Macromolecules* 47 (2014) 3701–3707, <https://doi.org/10.1021/ma500331w>.

- [15] E.J. Kim, J.M. Shin, Y. Kim, K.H. Ku, H. Yun, B.J. Kim, Shape control of nanostructured cone-shaped particles by tuning the blend morphology of a-b-b diblock copolymers and c-type copolymers within emulsion droplets, *Polym. Chem.* 10 (2019) 2415–2423, <https://doi.org/10.1039/C9PY00306A>.
- [16] H. Yang, K.H. Ku, J.M. Shin, J. Lee, C.H. Park, H.H. Cho, S.G. Jang, B.J. Kim, Engineering the shape of block copolymer particles by surface-modulated graphene quantum dots, *Chem. Mater.* 28 (2016) 830–837, <https://doi.org/10.1021/acs.chemmater.5b04222>.
- [17] J. Lee, K.H. Ku, C.H. Park, Y.J. Lee, H. Yun, B.J. Kim, Shape and color switchable block copolymer particles by temperature and pH dual responses, *ACS Nano* 13 (2019) 4230–4237, <https://doi.org/10.1021/acsnano.8b09276>.
- [18] K.H. Ku, H. Yang, J.M. Shin, B.J. Kim, Aspect ratio effect of nanorod surfactants on the shape and internal morphology of block copolymer particles, *J. Polym. Sci. Part A: Polym. Chem.* 53 (2015) 188–192, <https://doi.org/10.1002/pola.27333>.
- [19] J. Lee, K.H. Ku, M. Kim, J.M. Shin, J. Han, C.H. Park, G.-R. Yi, S.G. Jang, B.J. Kim, Stimuli-responsive, shape-transforming nanostructured particles, *Adv. Mater.* 29 (2017) 1700608, <https://doi.org/10.1002/adma.201700608>.
- [20] J.M. Shin, Y. Kim, H. Yun, G.-R. Yi, B.J. Kim, Morphological evolution of block copolymer particles: effect of solvent evaporation rate on particle shape and morphology, *ACS Nano* 11 (2017) 2133–2142, <https://doi.org/10.1021/acsnano.6b08342>.
- [21] J.M. Shin, Y. Kim, K.H. Ku, Y.J. Lee, E.J. Kim, G.-R. Yi, B.J. Kim, Aspect ratio-controlled synthesis of uniform colloidal block copolymer ellipsoids from evaporative emulsions, *Chem. Mater.* 30 (2018) 6277–6288, <https://doi.org/10.1021/acs.chemmater.8b01821>.
- [22] E.J. Kim, J.J. Shin, T. Do, G.S. Lee, J. Park, V. Thapar, J. Choi, J. Bang, G.-R. Yi, S.-M. Hur, J.G. Kim, B.J. Kim, Molecular weight dependent morphological transitions of bottlebrush block copolymer particles: experiments and simulations, *ACS Nano* 15 (2021) 5513–5522, <https://doi.org/10.1021/acsnano.1c00263>.
- [23] J.M. Shin, Y.J. Lee, M. Kim, K.H. Ku, J. Lee, Y. Kim, H. Yun, K. Liao, C.J. Hawker, B. J. Kim, Development of shape-tuned, monodisperse block copolymer particles through solvent-mediated particle restructuring, *Chem. Mater.* 31 (2019) 1066–1074, <https://doi.org/10.1021/acs.chemmater.8b04777>.
- [24] K.H. Ku, J.H. Ryu, J. Kim, H. Yun, C. Nam, J.M. Shin, Y. Kim, S.G. Jang, W.B. Lee, B.J. Kim, Mechanistic study on the shape transition of block copolymer particles driven by length-controlled nanorod surfactants, *Chem. Mater.* 30 (2018) 8669–8678, <https://doi.org/10.1021/acs.chemmater.8b04020>.
- [25] J. Lee, K.H. Ku, J. Kim, Y.J. Lee, S.G. Jang, B.J. Kim, Light-responsive, shape-switchable block copolymer particles, *J. Am. Chem. Soc.* 141 (2019) 15348–15355, <https://doi.org/10.1021/jacs.9b07755>.
- [26] J. Kim, H. Yun, Y.J. Lee, J. Lee, S.-H. Kim, K.H. Ku, B.J. Kim, Photoswitchable surfactant-driven reversible shape- and color-changing block copolymer particles, *J. Am. Chem. Soc.* 143 (2021) 13333–13341, <https://doi.org/10.1021/jacs.1c06377>.
- [27] D. Klinger, C.X. Wang, L.A. Connal, D.J. Audus, S.G. Jang, S. Kraemer, K.L. Killops, G.H. Fredrickson, E.J. Kramer, C.J. Hawker, A facile synthesis of dynamic, shape-changing polymer particles, *Angew. Chem.* 126 (2014) 7138–7142, <https://doi.org/10.1002/ange.201400183>.
- [28] K.H. Ku, Y.J. Lee, Y. Kim, B.J. Kim, Shape-anisotropic diblock copolymer particles from evaporative emulsions: experiment and theory, *Macromolecules* 52 (2019) 1150–1157, <https://doi.org/10.1021/acs.macromol.8b02465>.
- [29] E. Avalos, T. Teramoto, H. Komiyama, H. Yabu, Y. Nishiura, Transformation of block copolymer nanoparticles from ellipsoids with striped lamellae into onionlike spheres and dynamical control via coupled Cahn-Hilliard equations, *ACS Omega* 3 (2018) 1304–1314, <https://doi.org/10.1021/acsomega.7b01557>.
- [30] P. Chi, Z. Wang, B. Li, A.C. Shi, Soft confinement-induced morphologies of diblock copolymers, *Langmuir* 27 (2011) 11683–11689, <https://doi.org/10.1021/la202448c>.
- [31] R. Deng, F. Liang, W. Li, S. Liu, R. Liang, M. Cai, Z. Yang, J. Zhu, Shaping functional nano-objects by 3D confined supramolecular assembly, *Small* 9 (2013) 4099–4103, <https://doi.org/10.1002/smll.201300271>.
- [32] R. Deng, F. Liang, W. Li, Z. Yang, J. Zhu, Reversible transformation of nanostructured polymer particles, *Macromolecules* 46 (2013) 7012–7017, <https://doi.org/10.1021/ma401398h>.
- [33] R. Deng, H. Li, F. Liang, J. Zhu, B. Li, X. Xie, Z. Yang, Soft colloidal molecules with tunable geometry by 3D confined assembly of block copolymers, *Macromolecules* 48 (2015) 5855–5860, <https://doi.org/10.1021/acs.macromol.5b01261>.
- [34] M. Ren, Z. Hou, X. Zheng, J. Xu, J. Zhu, Electrostatic control of the three-dimensional confined assembly of charged block copolymers in emulsion droplets, *Macromolecules* 54 (2021) 5728–5736, <https://doi.org/10.1021/acs.macromol.1c00575>.
- [35] R. Deng, L. Zheng, X. Mao, B. Li, J. Zhu, Transformable colloidal polymer particles with ordered internal structures, *Small* 17 (2021) 2006132, <https://doi.org/10.1002/smll.202006132>.
- [36] R.R. Netz, D. Andelman, M. Schick, Interfaces of modulated phases, *Phys. Rev. Lett.* 79 (1997) 1058–1061, <https://doi.org/10.1103/PhysRevLett.79.1058>.
- [37] S. Cohen, D. Andelman, Interfacial phenomena of solvent-diluted block copolymers, *Macromolecules* 47 (2014) 460–469, <https://doi.org/10.1021/ma401479f>.
- [38] G.H. Fredrickson, E. Helfand, Fluctuation effects in the theory of microphase separation in block copolymers, *J. Chem. Phys.* 87 (1987) 697, <https://doi.org/10.1063/1.453566>.
- [39] S. Safran, *Statistical Thermodynamics of Surfaces, Interfaces, and Membranes*, Westview Press, Boulder, CO., 2003, <https://doi.org/10.1201/9780429497131>.
- [40] D. Hu, X. Chang, Y. Xu, Q. Yu, Y. Zhu, Light-enabled reversible shape transformation of block copolymer particles, *ACS Macro Lett.* 10 (2021) 914–920, <https://doi.org/10.1021/acsmacrolett.1c00356>.
- [41] J.G.E.M. Fraaije, B.A.C. van Vlimmeren, N.M. Maurits, M. Postma, O.A. Evers, C. Hoffmann, P. Altevogt, G. Goldbeck-Wood, The dynamic mean-field density functional method and its application to the mesoscopic dynamics of quenched block copolymer melts, *J. Chem. Phys.* 106 (1997) 4260–4269, <https://doi.org/10.1063/1.473129>.
- [42] S. Ji, R. Zhang, L. Zhang, Y. Yuan, J. Lin, Self-assembled nanostructures of diblock copolymer films under homopolymer topcoats, *Polym Int.* 69 (2020) 728–736, <https://doi.org/10.1002/pi.6009>.
- [43] C. Huang, Y. Zhu, X. Man, Block copolymer thin films, *Phys. Rep.* 932 (2021) 1–36, <https://doi.org/10.1016/j.physrep.2021.07.005>.
- [44] B. Xia, W.H. Li, F. Qiu, Self-assembling behaviors of symmetric diblock copolymers in C homopolymers, *Acta Chim. Sinica* 72 (2014) 30–34, <https://doi.org/10.6023/A13080892>.